CARBON 47 (2009) 1327–1334

available at www.sciencedirect.com

ScienceDirect

journal homepage: www.elsevier.com/locate/carbon

# Computation of the loading diagram and the tensile strength of carbon nanotube networks

*I. Zsoldos*[a,*], *I. Laszlo*[b]

[a]*Szent Istvan University, Faculty of Mechanical Engineering, Pater K. u. 1., H-2103 Godollo, Hungary*
[b]*Department of Theoretical Physics, Institute of Physics and Center for Applied Mathematics, Budapest University of Technology and Economics, H-1521 Budapest, Hungary*

ARTICLE INFO

*Article history:*
Received 19 June 2008
Accepted 12 January 2009
Available online 20 January 2009

ABSTRACT

A modification is suggested to the Brenner potential cut-off function in order to compute atomic forces of carbon nanostructures in a more realistic way and giving a possibility to fit the atomic forces to experimental data. With the modified Brenner potential, the loading diagram and the tensile strength were determined for an example of the carbon nanotube networks. According to these new computational results carbon nanotube networks can be the materials which inherit the extremely high strength of the graphite sheet and they bring this property in all directions of the 3D space (not only in one direction as the nanotubes).



## 1. Introduction

The $sp^2$ carbon–carbon bond in a graphite layer is the strongest of all chemical bonds in solids [1,2]. Theoretical strength values of the graphene were determined as $\sigma_C \cong 0.316$ TPa derived from Young's modulus [1,3] and $\sigma_T \cong 0.14$–$0.177$ TPa derived from the work of fracture [1,4,5]. This theoretical strength is important because it is the maximum theoretical strength for all solids.

The carbon nanotubes could be the materials which approach the theoretical strength of the graphene. Direct mechanical measurements of the tensile strength were carried out on multiwalled carbon nanotubes (MWCNC) [1,6] and on single wall carbon nanotube (SWCNT) ropes [7]. To determine the tensile strength a theoretical way was carried out by molecular mechanical calculations using different energetic potential functions. Different types of SWCNT-s were studied using primarily the empirical Brenner potential: [8–12]. For the same purpose, the Tersoff [9,13] and the Morse potential [12,11,14] were used, as well. Recently, the finite deformation shell theory was developed for theoretical studies of carbon nanotubes [15]. This continuum theory is based on use interatomic potential, as well, and it can be the next generation of theoretical methods to determine mechanical properties.

Accordingly, today the straight carbon nanotubes are the strongest materials. Nevertheless they show this property only in one direction. Their extremely high strength can be led by nanotube junctions into different directions of the three-dimensional (3D) space. The significance of nanotube junctions was first discovered in their electronic properties. For example a heterogeneous junction built from a zig-zag and an armchair tube behaves like a rectifying diode with nonlinear transport characteristics [16]. The current–voltage characteristics of a Y junction are measured [17], as well, and we may hope that the molecular transistor will be found in the group of the Y junctions. In our earlier research work we have defined a set of nanotube junctions built from armchair and zig-zag type straight tubes [18]. We have shown that any number of tubes having an optional diameter can be connected in a junction and we have developed a method to construct their models as well. Our system is created in such a

* *Corresponding author:* Fax: +36 28 522949.
E-mail address: zsoldos.ibolya@gek.szie.hu (I. Zsoldos).
0008-6223/$ - see front matter 
doi:10.1016/j.carbon.2009.01.017

way that if a tube of a given type is taken out from the junction, it can always be replaced with a contrary type one. This property can be interesting in electric applications. Later, we have presented that nanotubes of any chirality can be connected in a junction [19]. Nanotube junctions consisting of more than three tubes were observed in various experiments [20–22].

From different nanotube junctions different nanotube networks can be built. The basic types of regular networks are named as supersquare (the network constructed from X junctions), supergraphene (the honeycomb like network constructed from Y junctions), supercubic (the network constructed from junctions having six perpendicular tubes) and super-diamond (the network constructed from tetrahedral junctions) [21]. Several mechanical properties (Young's modulus, bulk modulus and deformation mechanisms) were determined for supersquares and supergraphenes [23]. Special fractal networks, so-called super-carbon nanotubes based on the nanotube structures were defined [24]. Others prognosticate a successful future for the random nanotube networks, although these networks have not contained junctions so far, only disordered tubes as dropping pickup sticks. They could be the most stable and the strongest electric conductors having almost zero failure probability. Researchers hope a new and cheap technology for their manufacturing will be found shortly. Several research institutes in the world prepare them today in plastic impregnated technology [22].

The goal of this work was to develop a method in order to calculate the loading diagram and the tensile strength of nanotube networks.

## 2. Calculational method

To determine the loading diagram and the tensile strength, atomic forces are needed to compute. The atomic forces can be calculated from a derived energetic potential function. For this purpose, we have chosen the empirical Brenner potential which is generally used in molecular mechanics and molecular dynamic studies not only in carbon nanostructures but in hydrocarbon structures, as well [25,26].

Brenner developed the interatomic potential for carbon as

$$V(r) = V_R(r) - \bar{B}_{ij} V_A(r_{ij}) \tag{1}$$

for atoms i and j, where $r = r_{ij}$ is the distance between atoms i and j. $V_R$ and $V_A$ are the repulsive and attractive terms given by

$$V_R = \frac{D_e}{S-1} e^{-\sqrt{2S}\beta(r-R)} f_{ij}(r_{ij}) \tag{2}$$

$$V_A = \frac{D_e S}{S-1} e^{-\sqrt{2/S}\beta(r-R)} f_{ij}(r_{ij}) \tag{3}$$

The so-called cut-off function $f_{ij}(r_{ij})$, which restricts the pair potential to the nearest neighbours, is given by

$$f_{ij}(r_{ij}) = \begin{cases} 1, & r_{ij} < R_1 \\ \left[1 + \cos\left(\frac{r_{ij}-R_1}{R_2-R_1}\pi\right)\right]/2 & R_1 \le r_{ij} \le R_2 \\ 0 & r_{ij} > R_2 \end{cases} \tag{4}$$

The parameter $B_{ij}$ in Eq. (1) represents a multibody coupling between the bond from atoms i and j and the local environment of atom i, and is given by

$$B_{ij} = \left[1 + \sum_{k(\neq i,j)} G(\theta_{ijk}) f_{ik}(r_{ik})\right]^{-\delta} \tag{5}$$

where $\theta_{ijk}$ is the angle between bonds i–j and i–k, and the function G is given by

$$G(\Theta) = a_0\left[1 + \frac{c_0^2}{d_0^2} - \frac{c_0^2}{d_0^2 + (1+\cos\Theta)^2}\right] \tag{6}$$

For atoms i and j that have a different local environment, Brenner suggested the replacement of the coefficient $B_{ij}$ in Eq. (1) by

$$\bar{B}_{ij} = (B_{ij} + B_{ji})/2 \tag{7}$$

In accord with our experience more authors have noticed that the cut-off function affects the computation of the atomic forces very strongly. It introduces a dramatic increase in the interatomic force at $r = R_1$ (like a camelback on the force curve), which rises sharply with a peak at around 30% strain, Fig. 1b. To avoid this problem Shenderova et al. shifted the cut-off function to larger strains so that it occurs after the inflexion point in the interatomic potential [27]. Belytschko et al. have found that the cut-off function affects strongly even when it is shifted to 100% strain [12]. Duan et al. assumed the cut-off function equal to 1 to avoid the dramatic increase in the interatomic force [11]. Mylvaganam et al. defined the changes of the slope on the interatomic force as different stages of the stress–strain curve [9].

Beside the above mentioned problem there are uncertainties in the measured and calculated strength values of carbon nanotubes, as well. In Table 1, we summarized the tensile strength values found in the literature. The values are rather different.

The reasons for the differences are partly because of the differences in the structures and partly because $\sigma_T$ is not defined the in same way by the authors.

To compute atomic forces in a more realistic way we suggest a modification in the cut-off function in the formulas of the Brenner potential. Fig. 1 shows the effect of the cut-off function on the energetic potential and on the atomic force curve in the case of only one chemical bond of the graphite sheet. The cut-off function ($f_{ij}$) is a monotonously decreasing curve, it decreases from 1 to 0 between the distances of $R_1$ and $R_2$, Fig. 1a. If we omit it from Brenner's formulas, the energetic potential approaches zero in the infinite, but if we do not leave it out, the curve approaches zero at $R_2$, Fig. 1b. The effect is stronger on the atomic force function: the curve computed with the cut-off function is basically other than the one without the cut-off function, Fig. 1b. Besides this there is a break point on the force curve, as well.

It is obvious that there is a large set of functions which keep the property of the original cut-off function: they decrease monotonously from 1 to 0 between $R_1$ and $R_2$, Fig. 2a. Consequently, if we use the elements of this set like cut-off function to compute the energetic potential and the atomic forces we can define a curve set for both of them, Fig. 2b. It is important to mention that a small change in the energetic potential curve between $R_1$ and $R_2$ means a large change in its derived function, in the atomic force curve. We suggest choosing the cut-off function from the function set in such

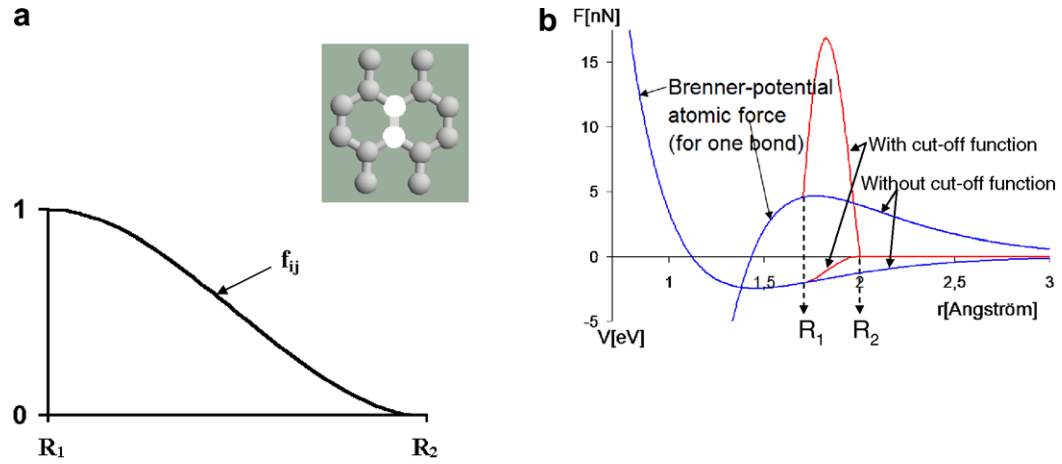


**Fig. 1 – The cut-off function (a) and its effect on the energetic potential and on the atomic force curve (b) in the case of only one chemical bond of the graphite sheet.**

**Table 1 – Experimental and calculated values of the tensile strength of different CNT-s**

| Nanotube structure | $\sigma_T$ (GPa) | Method |
|---|---|---|
| SWCNT ropes [7] | 13–50 | Loading experiment |
| MWCNT [6] | 11–63 | Loading experiment |
| MWCNT [1] | 150 | Loading experiment |
| (5,5) Nanotube [14] | 123 | Calculated with Morse potential |
| (9,0) Nanotube [14] | 94 | |
| (12,12) Nanotube [12] | 112 | Calculated with Morse potential |
| (16,8) Nanotube [12] | 106 | Calculated with Morse potential |
| (12,4) Nanotube [12] | 98 | Calculated with Morse potential |
| (20,0) Nanotube [12] | 93 | Calculated with Morse potential |
| (20,0) Nanotube [12] | 110 | Calculated with Brenner potential |
| (10,0) Nanotube [11] | 105.38 | Calculated with Morse potential |
| (10,0) Nanotube [11] | 99.89 | Calculated with Brenner potential |
| (10,1) Nanotube [11] | 106.09 | Calculated with Morse potential |
| (10,1) Nanotube [11] | 100.46 | Calculated with Brenner potential |
| (10,3) Nanotube [11] | 110.21 | Calculated with Morse potential |
| (10,3) Nanotube [11] | 102.59 | Calculated with Brenner potential |
| (10,5) Nanotube [11] | 116.83 | Calculated with Morse potential |
| (10,5) Nanotube [11] | 104.20 | Calculated with Brenner potential |
| (10,7) Nanotube [11] | 124.09 | Calculated with Morse potential |
| (10,7) Nanotube [11] | 104.93 | Calculated with Brenner potential |
| (10,9) Nanotube [11] | 130.93 | Calculated with Morse potential |
| (10,9) Nanotube [11] | 105.64 | Calculated with Brenner potential |
| (10,10) Nanotube [11] | 134.01 | Calculated with Morse potential |
| (10,10) Nanotube [11] | 111.93 | Calculated with Brenner potential |
| (10,10) Nanotube [9] | 1357 | Calculated with Brenner potential |
| (17,0) Nanotube [9] | 754 | |
| (14,14) Nanotube [10] | 250* | Calculated with Brenner potential |
| (24,0) Nanotube [10] | 125* | |
| (6,6) Nanotube [13] | 152.3 | Calculated with Tersoff potential |
| (8,3) Nanotube [13] | 107.6 | |
| (10,0) Nanotube [13] | 92.5 | |
| (5,5) Nanotube [8] | 1700–1800* | Calculated with Brenner potential |
| (9,0) Nanotube [8] | 1400* | |
| (10,10) Nanotube [8] | 1700–1800* | |
| (17,0) Nanotube [8] | 1400* | |
| (15,15) Nanotube [8] | 1700-1800* | |
| (26,0) Nanotube [8] | 1400* | |

* The value is read from the loading diagram.

a way that we fit the force curve to experimental results if it is possible. Beside this we suggest putting the value of $R_1$ to the minimum place of the energetic curve to avoid the breakpoint of the functions.

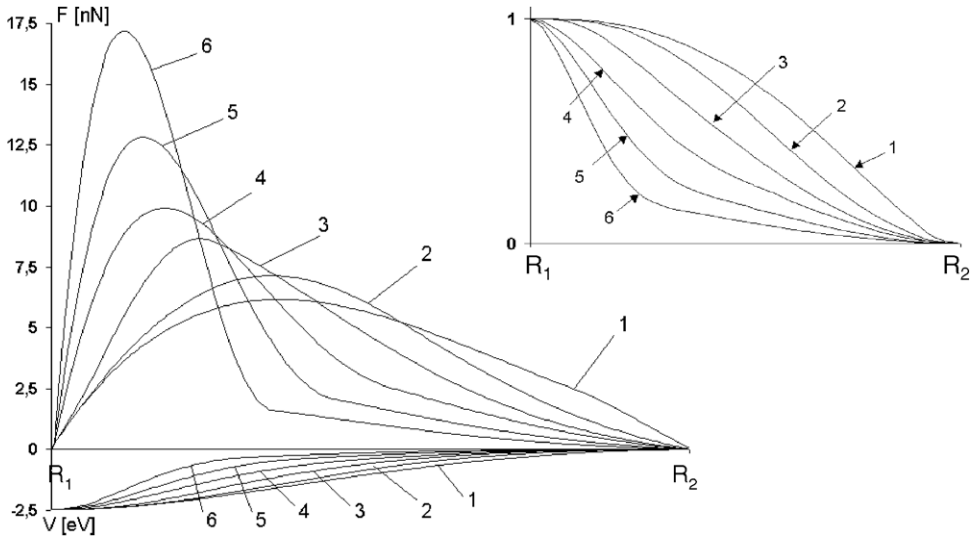


**Fig. 2 – (a) A set of the cut-off functions. (b) The energetic potential (lower half of the diagram) and the atomic forces (upper half of the diagram) computed with (6) different elements of the cut-off function set (for only one chemical bond of the graphite sheet).**

To describe the curve set of the cut-off function mathematically we used polynoms in two different intervals defined by

$$f_{ij}(r) = \begin{cases} f_1(r), R_1 \leqslant r \leqslant R_T \\ f_2(r), R_T < r \leqslant R_2 \end{cases} \quad (8)$$

where

$$f_1(r) = a_0 + a_1 r + a_2 r^2 + a_3 r^3 + a_4 r^4 \quad \text{and}$$
$$f_2(r) = b_0 + b_1 r + b_2 r^2 + b_3 r^3$$

The selection is favourable because polynoms are derived very easily. The two different intervals between $R_1$ and $R_2$ are separated by the inflexion point of the curve having coordinates of $R_T$ and $f_T$ which will be the free parameters for the fitting, Fig. 3.

The conditions to fit the curves at $R_1$, $R_2$ and $R_T$ determine nine different linear equations as

$$f_1(R_1) = 1 \quad (9)$$
$$f_1'(R_1) = d \quad (10)$$
$$f_1(R_T) = f_T \quad (11)$$
$$f_1'(R_T) = f_2'(R_T) \quad (12)$$
$$f_1''(R_T) = 0 \quad (13)$$
$$f_2(R_T) = f_T \quad (14)$$
$$f_2(R_2) = 0 \quad (15)$$
$$f_2'(R_2) = 0 \quad (16)$$
$$f_2''(R_T) = 0 \quad (17)$$

The role of the 'd' parameter in Eq.

The role of the 'd' parameter in Eq. (10) is to fit the force curve at $R_1$ to avoid the breakpoint if $R_1$ is not chosen to the minimum place of the energetic potential. Since we put $R_1$ to the minimum place, $d = 0$ in our calculations detailed in the Section 2.

The free parameters of $R_T$ and $f_T$ are intended to fit the potential function to experimental data. The tensile strength ($\sigma_T$) of several MWNTs is known from experiments today (see Table 1) and we will use one of these data for the fitting later (last paragraph of this chapter).

We mention here that the original version of the Brenner cut-off function, the cosine function can not be used in the fitting procedure because of the absence of free parameters.

We used a cubic and a fourth-degree polynom to solve the equation system (9)–(17).

In Eqs. (18)–(25), we show the solution of the nine equations for the coefficients of the polynoms. The recursive formulas can be used in computer codes very easily

$$b_3 = \frac{f_T}{2(R_2 - R_T)^3} \quad (18)$$
$$a_4 = \frac{3f_T - 3 - d(R_T - R_1) + 6b_3(R_2 - R_T)^2(R_T - R_1)}{(R_T - R_1)^4} \quad (19)$$
$$a_3 = \frac{4a_3[R_T^3 - R_1^3 - 3R_T^2(R_T - R_1)] + 3b_3(R_2 - R_T)^2 + d}{3(R_T - R_1)^2} \quad (20)$$
$$b_2 = -3b_3 R_T \quad (21)$$
$$a_2 = -3a_3 R_T - 6a_4 R_T^2 \quad (22)$$
$$a_1 = d - 2a_2 R_1 - 3a_3 R_1^2 - 4a_4 R_1^3 \quad (23)$$
$$b_1 = d - 2b_2 R_2 - 3b_3 R_2^2 \quad (24)$$
$$a_0 = 1 - a_1 R_1 - a_2 R_1^2 - a_3 R_1^3 - a_4 R_1^4 \quad (25)$$

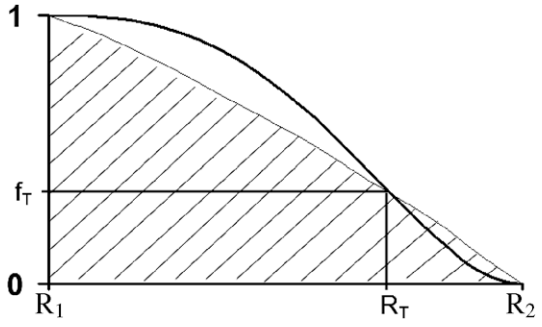


**Fig. 3 – The coordinates of the inflexion point $R_T$ and $f_T$ which will be the free parameters.**

The mathematical description of the curve set is not so easy. There are too many conditions (Eqs. (9)–(17)) and the solution for them is generally only partial. For example, let us regard the solution for an interval of $R_1 = 0.145$ nm and $R_2 = 0.2$ nm (this value was used everywhere in the literature). In this case we can choose values for $f_T$ and $R_T$ only inside a part of the rectangle defined by $(R_1,R_2)$ and (0,1) shown as the hatched area in Fig. 3. If the inflexion point is beyond this area, the monotonously decreasing property is not realized. However, the hatched area was enough to find the most applicable curve from the function set.

We fitted our parameters to experimental data calculated for one chemical bond. For this purpose, we have chosen Demczyk's et al. measurement on multiwalled nanotubes because the measured structure can be derived from their paper [1]. They observed a tensile force of 18 μN on a tube having a diameter of 12.5 nm, the type of the tube is not known. If we assume that the tube was a zig-zag type tube, then the outer tube has to have a (160,0) structure. The distance of the parallel tubes has to be minimum 0.34 nm which is the interlayer graphite distance, accordingly the inner tubes have to have (150,0), (140,0), (130,0), ..., (10,0) structures. It means that 160 + 150 + 140 + ... + 10 = 1360 bonds being parallel with the loading direction have to be broken together, so the tensile force is 18 μN/1360 = 13.23 nN for one bond. If we assume that the tube was an armchair type tube, then the outer tube has to have a (92,92) structure. The distance of the parallel tubes has to be minimum 0.34 nm which is the interlayer graphite distance, accordingly the inner tubes have to have (86,86), (80,80), (74,74), ..., (8,8) structures. It means that 2(92 + 86 + 80 + ... + 6) = 1500 bonds have to be broken together, the angle between the bonds and the loading direction is 30° at the beginning of the loading. Considering that the angle has to be a bit smaller at the tensile force, the tensile force has to be a bit smaller than 18 μN/1500/cos30° = 13.86 nN for one bond. To fit the maximum atomic force we have chosen 13.3 nN.

The strain value of the maximum force cannot be known in Demczyk's et al. paper [1] therefore we tried to compute without this.

In a special iteration procedure we varied the value of $R_T$ between $R_1$ and $R_2$ beside this we varied the value of $f_T$ between 0 and 1. It is obvious that for every value of $R_T$ we can find a value of $f_T$ so that the maximum force is the same, because we do not know the place of the maximum force. In this work, we selected four characteristic $(R_T,f_T)$ pairs in order to compute forces. The $(R_T,f_T)$ pairs with the corresponding atomic force and the energetic potential curves can be seen in Fig. 4. We mention again that in the case of a very small change in the energetic potential (see the fitted energetic functions in the lower part of the diagram) there is a large change in the atomic force function (see the fitted force functions in the upper part of the diagram: the change here is only in the place of the maximum force).

The maximum force on the fitted functions is smaller than the maximum one on the Brenner's original function, Fig. 4b, although we do not know how realistic our assumption is for the structure of the MWCNT in Demczyk's et al. experiment. The places of the maximum force, the tensile strain (6–12%) on the fitted functions are smaller than it is on Brenner's function (30%), as well, because we have shifted $R_1$ to the place of the minimum energy. For the tensile strain there are experimental results, as well: Yu et al. measured about 5% on SWCNT ropes [7] and about 10–12% on MWCNT [6], but we do not know it from Demczyk's et al. paper [1]. If there will be other or more accurate experimental data for the strain, it could be needed to fit the functions again and maybe to change $R_1$ and/or $R_2$. We notice that there can be smaller changes in the slope on the descending branch of the fitted atomic force curve in several cases (e.g. the dotted line in Fig. 4b), but this part of the atomic force function and that of any loading diagram is not important in engineering aspect.

In the end we mention that the values of $R_1$ and $R_2$ affect the maximum atomic force very strongly. Agrawal et al. showed differences in the loading diagram of nanotubes if $R_1$ is varied between 1.6 and 1.7 [10]. In our calculation, $R_1$ equals to the equilibrium atomic distance in unloaded state to avoid the break point on the atomic force curve. The physical mean of a slope–change on the curve is not known. $R_2$ is the same as Brenner's original value.

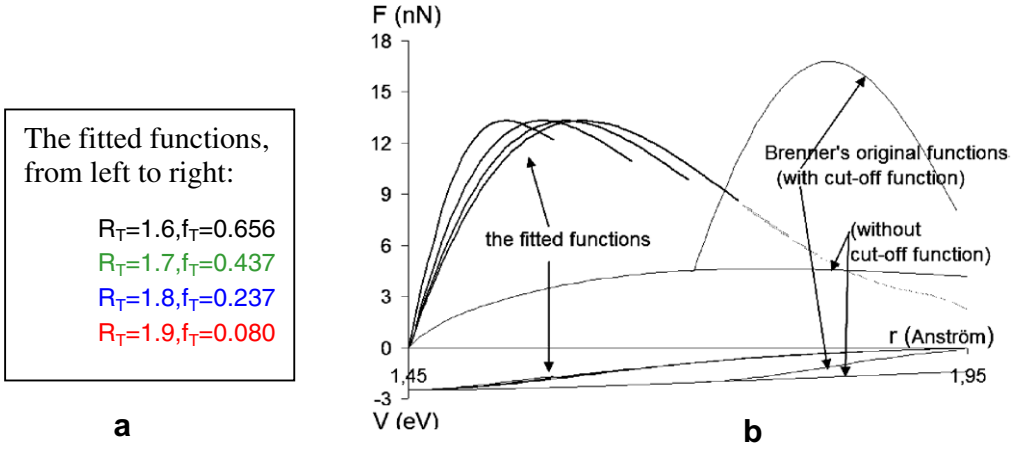


**Fig. 4 – (a) $(f_T,R_T)$ pairs, (b) the corresponding atomic force (*F* in nN-s, upper part) and the energetic potential curves (*V* in eV-s, lower part) fitted to experimental data in case of one chemical bond (*r* is the bond distance).**

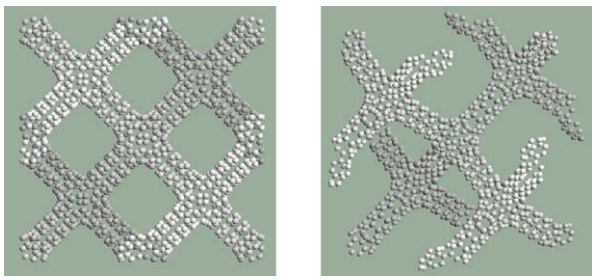

**Fig. 5 – Different views of the unit cell of the selected network.**

For the energetic potential we used the second set of parameters provided by Brenner adopted here as follows:

$D_e = 0.9612$ nN nm, $S = 1.22$, $\beta = 21$ nm$^{-1}$, $R = 0.139$, $\delta = 0.5$, $a_0 = 0.00020813$, $c_0 = 330$, $d_0 = 3.5$, $R_1 = 0.17$ nm, $R_2 = 0.2$ nm.

This set corresponds to the equilibrium bond length $r_0 = 0.145$ nm.

In order to compare our method with other works (see in Table 1), we have calculated the tensile strength of a zig-zag (10,0) and an armchair (10,10) tube in the case of the four selected ($R_T$,$f_T$) pairs. In these calculations, we have divided the maximum force calculated from the loading process (parallel with the tube axis) by the cross section of the tubes given by $D\pi t$ where $D$ is the diameter of the tube and $t = 0.34$ nm is the interlayer graphite distance. We have found that the tensile strength of the (10,0) tube is 156 GPa for all the four ($R_T$,$f_T$) pairs and the corresponding strain is between 5% and 13%, the tensile strength of the (10,10) tube is 178 GPa for all the four ($R_T$,$f_T$) pairs and the interval of the corresponding strain is a bit greater than it is for the (10,0) tube. The order of magnitude of these values is the same as Duan's et al. [11], Belytschko's et al. [12] and Agrawal's et al. [10] results. Our $\sigma_T$ values are greater than Duan's et al. [11] and Belytschko's et al. [12] results where the cut-off function is omitted from the calculations, and smaller than Agrawal's et al. [10] results where the second generation of the Brenner potential [26] was applied. The tendency that an armchair type tube is stronger

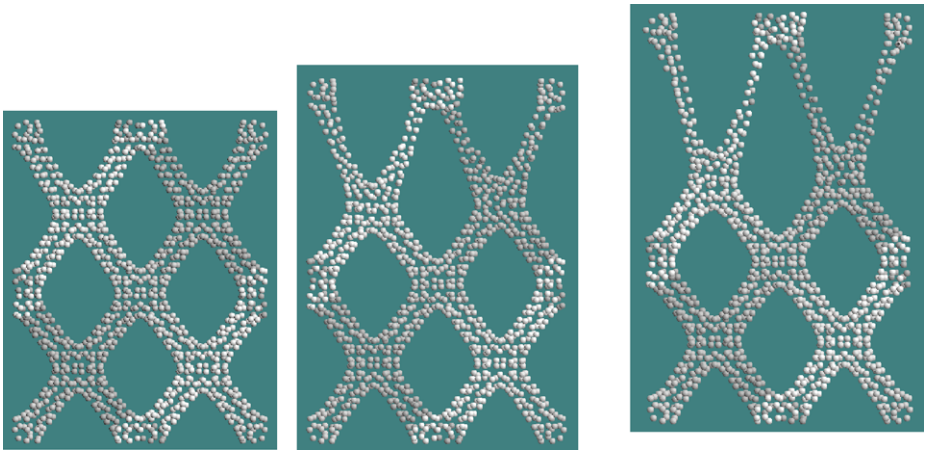

**Fig. 6 – The structure after 28%, 40% and 55% elongation.**

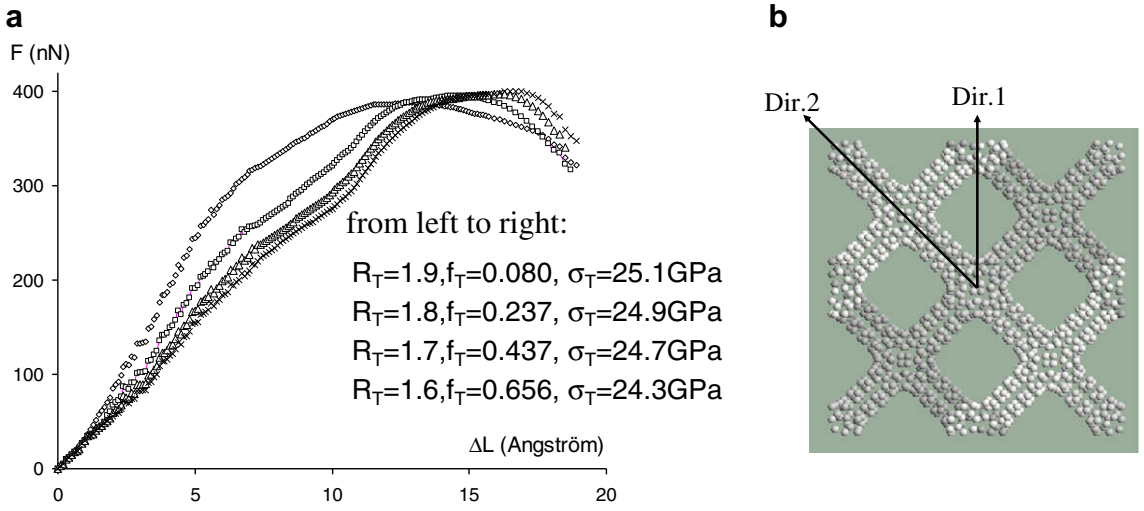


**Fig. 7 – The loading diagrams and the tensile strength (a) for the first loading direction (b).**

than a zig-zag type tube is similar in our calculation to the one Duan's et al. [11] work, where the chirality dependence of nanotubes was studied.

## 3. Calculated results

The aim of this work was to determine the strength properties of carbon nanotube networks. A super-diamond structure consisting of (3,3) nanotubes was selected for our computation. In Fig. 5, we can see the 1186 atom initial unit cell of 39.94 Å. During our calculations we kept periodic boundary condition.

The loading simulation was carried out by elongating the structure in very small steps. After each step, we computed the new equilibrium positions of the carbon atoms. We noticed for the equilibrium coordinates that any cut-off functions of our set gave the same result as the original one. Namely the modified cut-off function does not change the minimum place of the energetic potential. In Fig. 6, the three snapshots of the simulation show the structure after 28%, 40% and 55% elongation. It can be seen that the structure starts to break at the straight tubes and not at the junctions.

In the end we calculated the loading diagrams using the four selected ($R_T$,$f_T$) pairs to compute atomic forces detailed in the Section 1. To determine the tensile strength we divided the maximum force by the cross section of the unit cell. We carried out the computations for two main directions, Fig. 7b. The loading diagram and the calculated tensile strength for the direction being perpendicular to the faces of the unit cell (Dir. 1) can be seen in Fig. 7a. If the loading direction is parallel with the tube axes (Dir. 2), the value of the tensile strength was a bit smaller: 20.2, 20.7, 21.1 and 21.4 GPa for the selected ($R_T$,$f_T$) pairs of (1.6, 0.656), (1.7, 0.437), (1.8, 0.237), (1.9, 0.080), respectively.

Thus the tensile strength is between 24.3 and 25.1 GPa and the corresponding strain is between 20% and 50% for the direction which is perpendicular to the faces of the unit cell. Similarly, the tensile strength is between 20.2 and 21.4 GPa and the corresponding strain is between 20% and 50% for the direction which is parallel with the tube axes. To sum up the difference in the tensile strength between our network and the single nanotubes is less than one order of magnitude, and we mention beside the above that our example is not the densest network.

## 4. Conclusions

As the cut-off function of our modified Brenner potential was fitted to experimental loading data it can be applied in a more realistic way in order to compute the loading simulations and characteristic forces of various carbon nanostructures.

Carbon nanotube networks can be the materials which inherit the extremely high strength of the graphite sheet and they bring this property in all directions of the 3D space (not only in one direction as the nanotubes).

## Acknowledgement

This work was supported by OTKA grants K 73776 in Hungary.

## REFERENCES

[1] Demczyk BG, Wang YM, Cumings J, Hetman M, Han W, Zettl A, Ritchie RO. Direct mechanical measurement of the tensile strength and elastic modulus of multiwalled carbon nanotubes. Mater Sci Eng A 2002;334:173–8.
[2] Coulson CA. Valence. Oxford: Oxford University Press; 1952.
[3] Kelley BT. Physics of Graphite. Applied Science. London; 1981.
[4] Polanyi M. Uber die Natur des Zerreissvorgangenes. Z Phys 1921;7:323–7.
[5] Orowan E. Fracture and strength of solids. Rep Prog Phys 1949;12:185–232.
[6] Yu MF, Lourie O, Dyer MJ, Moloni K, Kelly TE, Ruoff RS. Strength and breaking mechanism of multiwalled carbon nanotubes under tensile load. Science 2000;287:637–40.
[7] Yu MF, Files BS, Arepalli S, Ruoff R. Tensile loading of ropes of single nanotubes and their mechanical properties. Phys Rev Lett 2000;84:5552–5.
[8] Fu CX, Chen YF, Jiao JW. Molecular dynamics simulation of the test of single-walled carbon nanotubes under tensile loading. Sci China E 2008;50:7–17.
[9] Mylvaganam K, Zhang LC. Important issues in a molecular dynamics simulation for characterising the mechanical properties of carbon nanotubes. Carbon 2004;42:2025–32.
[10] Agrawal PM, Sudalayandi BS, Raff LM, Komanduri R. Molecular dynamic (MD) simulations of the dependence of C–C bond lengths and bond angles on the tensile strain in single-wall carbon nanotubes (SWCNTs). Comput Mater Sci 2008;41:450–6.
[11] Duan WH, Wang Q, Liew KM, He XQ. Molecular mechanics modelling of carbon nanotube fracture. Carbon 2007;45:1769–76.
[12] Belytschko T, Xiao SP, Schatz GC, Ruoff R. Atomistic simulations of nanotube fracture. Phys Rev B 2002;65:235430-1-8.
[13] Jeng YR, Tsai PC, Fang TH. Effects of temperature and vacancy defects on tensile deformation of single-walled carbon nanotubes. J Phys Chem Solids 2004;65:1849–56.
[14] Meo M, Rossi M. Tensile failure prediction of single wall carbon nanotube. Eng Fract Mech 2006;73:2589–99.
[15] Wu J, Hwang KC, Huang Y. An atomistic-based finite-deformation shell theory for single-wall carbon nanotubes. J Mech Phys Solids 2008;56(1):279–92.
[16] Yao Z, Postma HWCh, Balents L, Dekker C. Carbon nanotube intramolecular junctions. Nature 1999;402:273–6.
[17] Bandaru PR, Daraio C, Jin S, Rao AM. Novel electrical switching behaviour and logic in carbon nanotube Y junctions. Nat Mater 2005;4:663–6.
[18] Zsoldos I, Kakuk G, Reti T, Szasz A. Geometric construction of carbon nanotube junctions. Modelling Simul Mater Sci Eng 2004;12:1–16.
[19] Laszlo I. Construction of atomic arrangement for carbon nanotube junctions. Phys Stat Sol 2007;244:4265–8.
[20] Ting JM, Li TP, Chang CC. Carbon nanotubes with 2D and 3D multiple junctions. Carbon 2004;42:2997–3002.
[21] Romo-Herrera JM, Terrones M, Terrones H, Dag S, Meunier V. Covalent 2D and 3D networks from 1D nanostructures: designing new materials. Nanoletters 2007;7:570–6.
[22] Graner G. Carbon nanonets spark new electronics. Sci Am 2007;5:58–65.
[23] Coluci VR, Dantas SO, Jorio A, Galvao DS. Mechanical properties of carbon nanotube networks by molecular mechanics and impact molecular dynamics calculation. Phys Rev B 2007;75:075417-1-7.
[24] Coluci VR, Galvao DS, Jorio A. Geometric and electronic structure of carbon nanotube networks: 'super'-carbon nanotubes. Nanotechnology 2006;17:617–21.

[25] Brenner DW. Empirical potential for hydrocarbons for use in simulating the chemical vapor deposition of diamond films. Phys Rev B 1990;42:9458–71.
[26] Brenner DW, Shenderova OA, Harrison JA, Stuart SJ, Ni B, Sinnott SB. A second- generation reactive empirical bond order (REBO) potential energy expression for hydrocarbons. J Phys 2002;14:783–802.
[27] Shenderova OA, Brenner DW, Omeltchenko A, Su X, Yang LH. Atomistic modeling of the polycrystalline diamond. Phys Rev B 2000;61:3877–88.